Chapter 5
Laser Additive Manufacturing of Single-Crystal Superalloy Component: From Solidification Mechanism to Grain Structure Control

Chaoyue Chen, Jiang Wang, Hanlin Liao, Zhongming Ren, and Shuo Yin

5.1 Introduction

Nickel-based superalloys are materials of choice for manufacturing the hot-section components in the gas turbine due to their superior mechanical properties at high temperatures (Han et al. 2019; Luo et al. 2019). Notably, the nickel-based superalloys in the form of single crystal (SX) are manufactured through directional solidification techniques to obtain one single grain in the whole component. Compared with polycrystalline alloys, the superior creep and thermal fatigue resistance can be obtained for the SX superalloy through the absence of grain boundaries (Anderson et al. 2010; Vitek 2005). As a result, the SX superalloys have been widely applied as the desired material selections for the high-temperature turbine section of aero and industrial gas turbine engines (Kong et al. 2019; Inaekyan et al. 2019; Wang and Chou 2017). However, the SX superalloy parts will experience unavoidable damage under the extremely severe service environment with high temperature, high pressure, and severe corrosion. Due to the high manufacturing cost of such SX components, the effective repair techniques for the damaged SX superalloy are highly desired to extend the service life of the hot-section components, such as blades, blisks, and vane seal segments. For this moment, the popular welding techniques

C. Chen · J. Wang · Z. Ren
State Key Laboratory of Advanced Special Steels, School of Materials Science and Engineering, Shanghai University, Shanghai, China
e-mail: cchen1@shu.edu.cn; jiangwang@i.shu.edu.cn; zmren@shu.edu.cn

H. Liao
ICB UMR 6303, CNRS, Univ. Bourgogne Franche-Comté, UTBM, Belfort, France
e-mail: hanlin.liao@utbm.fr

S. Yin (✉)
Department of Mechanical and Manufacturing Engineering, Trinity College Dublin, The University of Dublin, Dublin 2, Ireland
e-mail: yins@tcd.ie

© Springer Nature Switzerland AG 2021

P. Cavaliere (ed.), *Laser Cladding of Metals*,
https://doi.org/10.1007/978-3-030-53195-9_5

like TIG with high energy input and high-thermal-affected area cannot avoid the formation of stray grain as well as cracks within the repaired SX component (Gäumann et al. 1999; Basak and Das 2016; Chauvet et al. 2018a).

Among the various methods, laser additive manufacturing (LAM) has become an effective technique to realize the repair of damage SX components (Vilar and Almeida 2015; Gäumann et al. 2001). The high-energy laser beam is used to melt the feedstock metals to form the molten pool, whereas the feedstock materials can be the powder bed, powder feeding, and the wires (Herzog et al. 2016; Körner 2016; DebRoy et al. 2018). Due to the small spot size and high energy density, the LAM technique can achieve the damage repair with limited heat-affected zone and low distortion caused by thermal stress (Li et al. 2019). Coordinated with the industrial robot, the high-resolution LAM technique is able to realize the repair and restoration of the damaged components with complex geometry. However, due to the complex melting and solidification process, the columnar growth in the LAM process cannot be precisely controlled to obtain the SX structure. During this process, if specific solidification conditions are satisfied, the epitaxial growth of columnar cells/dendrites along the original orientation in the substrate occurs, and no equiaxed stray grains (SGs) will form. Otherwise, columnar-to-equiaxed transition (CET) takes place, and equiaxed SGs are produced, indicating the failure of the repairing process. Thus, the processing parameters should be carefully chosen to obtain the desired epitaxial growth of single-crystalline alloys based on the SX substrate so as to realize the repair of the SX turbine blade and make a right consistency of the mechanical properties between the repaired and substrate regions.

Existing work mainly focused on the solidification mechanism, processing parameter optimization, and cracking development. So far, a systematic summarization and review of these topics are still lacking. Therefore, in this chapter, the existing work on the LAM of SX superalloys was summarized and reviewed for the purpose of systematically introducing the recent progress.

5.2 Laser Additive Manufacturing Techniques

Different from the traditional subtraction manufacturing, the metallic additive manufacturing (AM) is a novel technology that joins materials to generate three-dimensional parts directly from CAD models based on the discrete-stacking principle (Han et al. 2019; Luo et al. 2019; Anderson et al. 2010; Vitek 2005; Kong et al. 2019; Inaekyan et al. 2019). Metallic AM techniques have various eye-catching advantages in comparison with other manufacturing technologies, such as the freedom of design and manufacturing, a short manufacturing cycle, and less material waste (Wang and Chou 2017; Gäumann et al. 1999). In addition, metallic AM technology has spread into various fields, such as the mold industry (Basak and Das 2016), the aerospace (Chauvet et al. 2018a), automotive fields (Vilar and Almeida 2015), etc.

Recently, the powder bed fusion (PBF) method has become the most distinguished metallic AM technique, including selective laser melting (SLM) (Yan et al. 2018, 2019) and selective electron-beam melting (SEBM) (Herzog et al. 2016). It is worth noting that SLM technology is more easily applied in the fabrication of metallic molds that have conformal cooling channels and functional parts with complicated geometries. Such unique advantages can be attributed to its flexibility in geometric design, high spatial resolution, and smaller amounts of material waste (Körner 2016; DebRoy et al. 2018).

This method can either flexibly add alloying elements (laser surface alloying) to the molten pool during the rapid melting or directly melt the alloy powder (laser cladding) that is simultaneously conveyed on the surface of the part to solidify quickly (Herzog et al. 2016; Gu et al. 2013; King et al. 2015). It is able to obtain the coating material with the characteristics of fine and uniform rapid solidification and nonequilibrium structure, which is different from the composition of the substrate material. It can also directly integrate material design, material preparation, and rapid near-net forming to produce complex structural parts. Laser additive manufacturing can adjust the solidification structure by adjusting the process parameters, not only the small equiaxed crystal structure but also the long columnar crystal structure epitaxially grown from the substrate (Basak and Das 2016). Thus, the integration from material composition and structural design to part manufacturing and forming is genuinely realized. Therefore, additive manufacturing is hailed as a representative technology that is expected to become the "third industrial revolution" and is a leading technology for the development of mass-production models to personalized manufacturing models.

At present, the most representative of laser additive manufacturing technology is selective laser melting (SLM), with powder bed as the technical feature, and laser direct metal deposition (LDMD), with synchronous powder feed as the technical feature. As shown in Fig. 5.1a, SLM technology is based on selective laser sintering (SLS) technology (Herzog et al. 2016; Dadbakhsh et al. 2014). Due to the development and application of high-power lasers, SLM technology can completely melt powder particles. In addition, the powder size of the SLM technology is smaller, and the laser beam with a smaller spot size is used, so the surface accuracy of the formed part is higher. However, due to the limitation of the printing chamber, SLM can only process precision parts with small size and complicated structure and cannot manufacture some large integral metal components. As shown in Fig. 5.1b,c, the LDMD technology is based on laser cladding technology (Yan et al. 2014; Ren et al. 2017). It is not limited by the fabrication chamber and can manufacture some large-sized metal components. Besides, it can control the process parameters to achieve the directional growth of the metal structure to prepare columnar crystal structure and single-crystal structure to achieve the effect of rapid repair of damaged parts. In addition, functionally graded composite materials and metal-based composite materials can be prepared by mixing different materials.

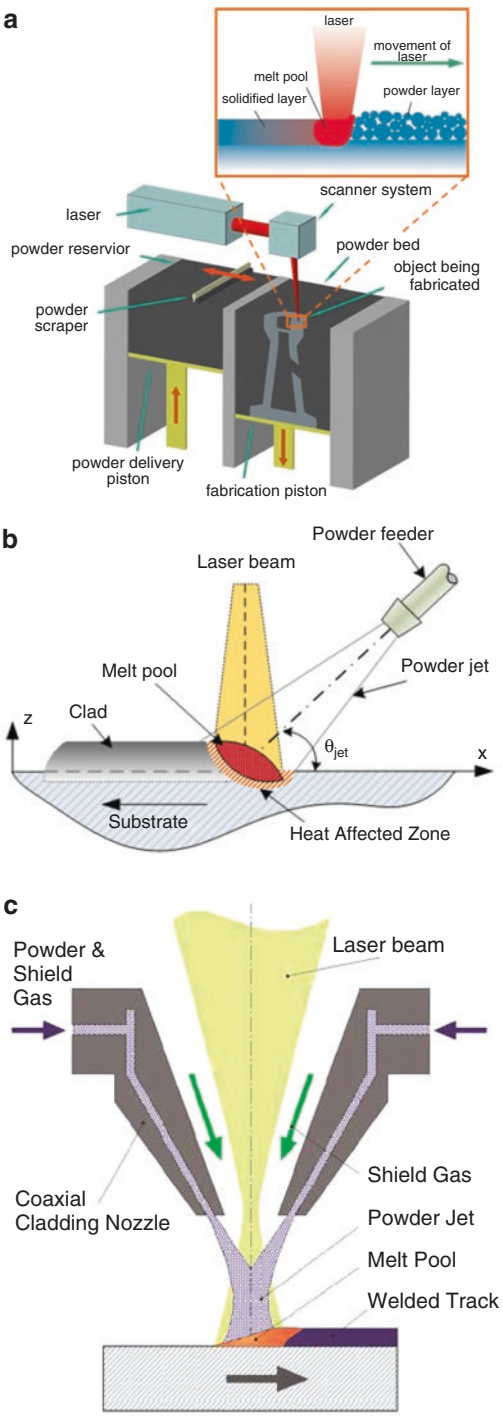

Fig. 5.1 Schematic diagram of laser additive manufacturing process: (**a**) SLM; (**b**) side powder feed LDMD; (**c**) coaxial powder feed LDMD

5.3 Solidification Mechanism of SX via AM

In order to obtain the single-crystal solidification during the laser additive manufacturing process, the key is to find the relation between the processing parameters and the solidification structure. Characterized by the high cooling rate and thermal gradient, the laser additive manufacturing presents distinct solidification features from the traditional solidification processes. For both the LAM of polycrystalline and the epitaxial growth of single-crystalline alloys, enormous efforts have been attributed to reveal the solidification structure diagram according to the temperature gradient and growth rate as well as the processing parameters.

For example, in AM Ti6Al4V samples by laser or electron beam, the columnar prior β grain is found to dominate the solidified microstructure, leading to the strong microstructural textures and anisotropy of the mechanical properties (Ren et al. 2017; Liu and Shin 2019). Similarly, the columnar grain morphology composed of γ phases is dominating the AM Ni-based superalloys along the building direction, leading to a typical attributed <001> texture (DebRoy et al. 2018; Hosseini and Popovich 2019). Such epitaxially growing columnar crystal from the substrate material or previously deposited layer is mainly due to the extremely high thermal gradient along the building direction during laser additive manufacturing. However, under certain thermal conditions, the epitaxially growing columnar structure can be interrupted and replaced by the formation of equiaxed grains. Such columnar-to-equiaxed transition (CET) occurs when nucleation of sufficiently numerous equiaxed dendrites takes place in the constitutionally undercooled liquid adjacent to the columnar dendritic front. The stability of the solidification front is controlled by the extent of the constitutional undercooling ahead of the advancing interface. Such stability is influenced by the presence of alloying or impurity elements, local grain growth rate, R, and the thermal gradient in the molten pool, G. As shown in Fig. 5.2, the higher ratio between G and R, namely, the G/R, results in a planar solidification front. At lower G/RL ratios, the morphology changes to cellular, cellular-dendritic, or dendritic, depending on the constitutional undercooling at the advancing solidification front (see Fig. 5.2). Thus, for the given material system with specific element composition, the grain morphology, as well as the CET, is mainly determined by the ratio between thermal gradient of G and solidification velocity of R. A fully columnar structure can be obtained at a sufficiently G/R value, while the equiaxed grains are emerging as the value G/R is higher than a critical value.

Figure 5.3 shows a typical cross-sectional microstructure of the laser-deposited CMSX-4 sample on a single-crystal substrate (Acharya et al. 2014). It can be seen that the epitaxial growth dendrite along the [001] direction. However, it is also evident that the CET was formed at the top of the deposited layer, where the stray grain formation appears as misoriented and equiaxed grains in the deposited microstructure. The control of CET and suppression of stray grain formation become the major challenges for the manufacturing of SX superalloy via the LAM technique. As shown in Fig. 5.4, the variation of solidification speed V and thermal gradient G is illustrated within the molten pool along the building direction of the z-axis

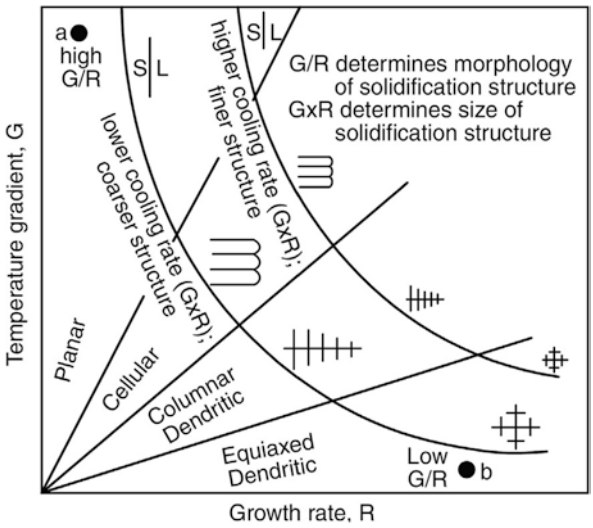

Fig. 5.2 Effect of temperature gradient G and growth rate R on the morphology and size of solidification microstructure (Kou 2003)

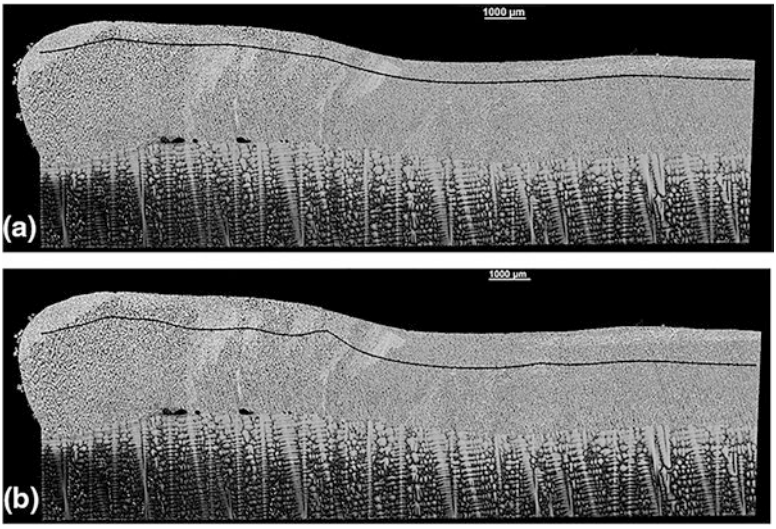

Fig. 5.3 Representative CMSX-4 sample (**a**) with the CET initiation indicated by the black line and (**b**) showing termination of [001] growth to [100] growth or OMT (Acharya et al. 2014)

(Gäumann et al. 1999). It can be seen that the solidification speed of V rapidly increases from zero at the bottom to the maximum value at the surface of the molten pool. On the contrary, the temperature gradient G is highest at the bottom of the molten pool, which gradually decreases as the surface is approached. As a result, the epitaxial growth of columnar dendrites is most likely to form from the molten pool, whereas the stray grains can be formed with the ratio of G/V that gradually decreases with the deposition process. The key is to control the vulnerable to columnar-to-equiaxed transition (CET) process of Ni-based SX superalloy by revealing the

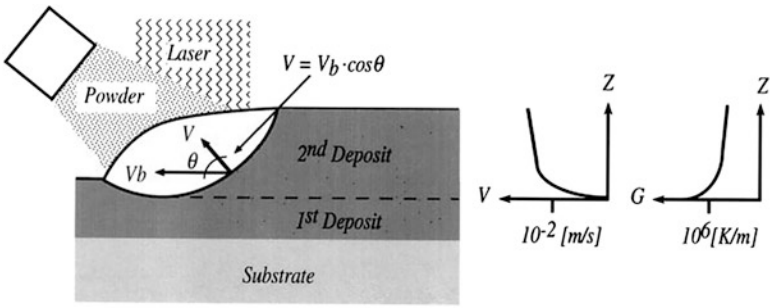

Fig. 5.4 Schematic longitudinal section along the clad centerline presenting the laser metal-forming process and the evolution of the solidification velocity *V* and temperature gradient *G* along with the solid/liquid interface (Gäumann et al. 1999)

relation between thermal history (thermal gradient and solidification speed) and epitaxial solidification model in the rapid solidification process of LAM.

In order to better control the epitaxial growth of the single crystal from an SX substrate, enormous efforts have been made to predict the CET with a quantitative equation to describe the relation between *G* and *R* (Gäumann et al. 2001; Liang et al. 2016, 2017a, b). It is then able to obtain the solidification structure from columnar to equiaxed grains in the LAM materials by controlling the processing parameters like laser powder and scanning speed. To quantitatively investigate this crucial phenomenon prevalent in solidification, Hunt (1984) developed the first analytical CET model for the casting process based on the growing competition between columnar dendrites and new equiaxed grains at the solidification front. At the sufficient constitutional supercooling, the mechanism of stray grain formation in the casting process is the nucleation and growth of equiaxed grains ahead of the solidification interface, which is determined by the ratio between thermal gradient and solidification velocity. Hunt proposed that the fully equiaxed growth occurs if the volume fraction of equiaxed grains Φ is higher than 49%, whereas the structure is becoming entirely columnar if Φ is lower than 0.66%. In order to quantitatively describe the CET model of the laser melting process, Gäumann et al. (1999, 2001) subsequently adapted the Hunt's model to the rapid solidification conditions by using the Kurz-Giovanola-Trivedi (KGT) model (Kurz et al. 1986). Gäumann found that the constitutional undercooling at the solidification front is the dominant factor for the CET at a lower thermal gradient and lower solidification velocity, which means that the formation of equiaxed grains is more easily to be triggered at a lower nucleation undercooling degree. However, the quantity of nucleation sites plays a more vital role in the case of rapid solidification cases with higher thermal gradients. Thus, to easily relate CET to the solidification conditions, a simplified CET criterion for complex multicomponent alloys was further derived (Gäumann et al. 2001):

$$\frac{G^n}{v} = K_{\mathrm{CET}} = \alpha \left[\sqrt[3]{\frac{-4\pi N_0}{3\ln(1-\phi)}} \times \frac{1}{n+1} \right]^n \tag{5.1}$$

where G is the thermal gradient, v is the solidification velocity, N_0 is nuclei density, Φ is the fraction of equiaxed grains, and a and n are the material-dependent constants. While the G^n/v is higher than the critical value of K_{CET}, the CET will be triggered during the laser additive manufacturing process. As shown in Fig. 5.5, the microstructure selection map for superalloy CMSX-4 under the experimental conditions is illustrated to predict the solidification morphology as a function of temperature gradient, G, and solidification velocity, V. For example, a microstructure selection map of superalloy CMSX-4 for a nuclei density $2 \times 10^{15}/m^3$ was built to predict the formation of columnar and equiaxed structure (Gäumann et al. 2001). It should be noted that CET is critical to the quality of the single-crystal deposit because it limits the height of columnar dendrite growth. The rectangular insert shows the range of conditions which is typical for the LMF process.

Besides, it should be noticed that the different LAM techniques present distinct microstructure selection patterns due to their thermal history. As can be seen in Fig. 5.6, the selective laser melting (SLM) presents a notably higher G/V ratio than

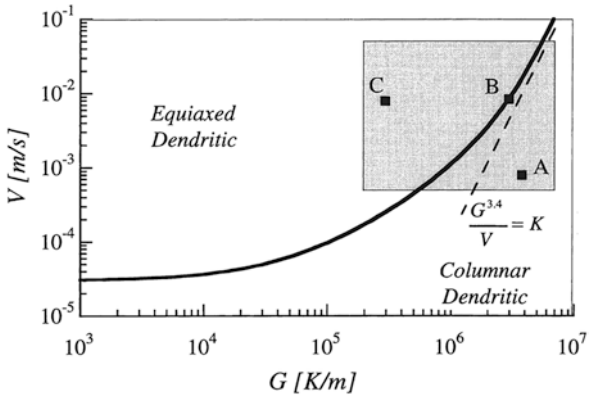

Fig. 5.5 Microstructure selection map for superalloy CMSX-4 (Gäumann et al. 1999)

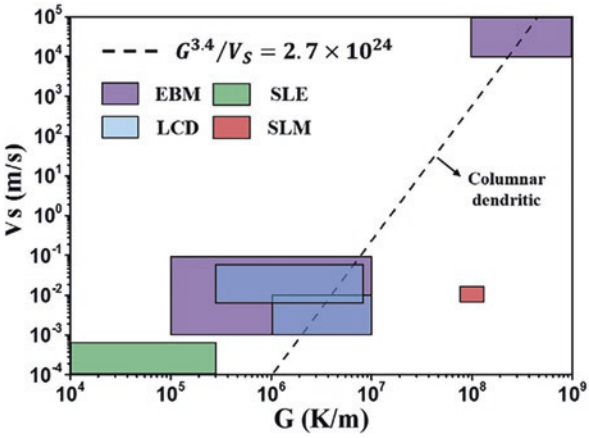

Fig. 5.6 Comparison of G and Vs among several kinds of LAM technologies (Yang et al. 2019)

the methods like laser cladding deposition due to its higher energy density with a smaller laser spot size (around 100 μm). Thus, the SLM can be another potential technique to realize the fabrication of the SX superalloy component. However, the control of the columnar misorientation angle becomes the key challenge under the complex laser scanning strategy.

5.4 Influence of Laser Processing Parameters

M. Gäumann et al. (1999, 2001) reported the first attempt to fabricate the single-crystal deposits using the epitaxial laser metal forming. Figure 5.7 shows the cross-sectional morphology of a CMSX-4 deposit on the single-crystal substrate, where the left column is the OM (optical microscopy) images and the right one is the EBSD patterns. From both the OM and EBSD images, it is evident that the deposit shows a columnar dendritic structure at the bottom of the deposit. Meanwhile, the equiaxed grains can be observed at the top of the layer indicating the CET occurrence, which is induced due to the insufficient thermal gradient as the LAM process (Fig. 5.8).

Various researchers have made vast efforts on the epitaxial growth of the SX superalloy under different processing parameters. Santos et al. (2011) used the laser metal deposition to fabricate the SX CMSX-4 deposit on the Rene N4 substrate. By optimizing the processing parameter and deposition orientation, the SX deposit layer was obtained on the substrate, whereas the height of the SX region can occupy 30–40% of each deposited layer. As shown in Fig. 5.9, the deposit layer growth epitaxially from the substrate along the [001] direction, which is the same as the maximum thermal gradient. It is obvious that the CET occurred at the top layer of deposit (see Fig. 5.9), where the equiaxed grain was formed along the [100] direction. However, during the continuous deposition process, the equiaxed grain region can be remelted, and the epitaxial growth can be continued from the columnar region to form the subsequent SX deposit layer. Thus, the crystallographic orientation of the SX structure can be preserved across the successive layers. As shown in Fig. 5.9, the CMSX-4 sample composed of ten layers of epitaxial growth can be obtained with the misorientation different from the less than 2°. Meanwhile, it is also evident that the interior columnar structure was surrounded by the equiaxed grains at the exterior of the sample.

In order to predict the epitaxial growth of the dendritic grains based on the SX substrate, Liu and Qi (2014, 2015a) established a three-dimensional finite element model to simulate the temperature field of the direct laser deposition. The effects of laser power, scanning speed, and powder feeding rate were accounted for in the finite element simulation and the experimental investigations. It is found that the processing parameters can directly determine the shape of the molten pool and, in turn, affected the epitaxial growth features of the deposited layer. As can be seen in Fig. 5.10a–c, at the laser power of 300 W, the height ratio between the epitaxial columnar dendritic region and that of the total deposit along the [001] orientation

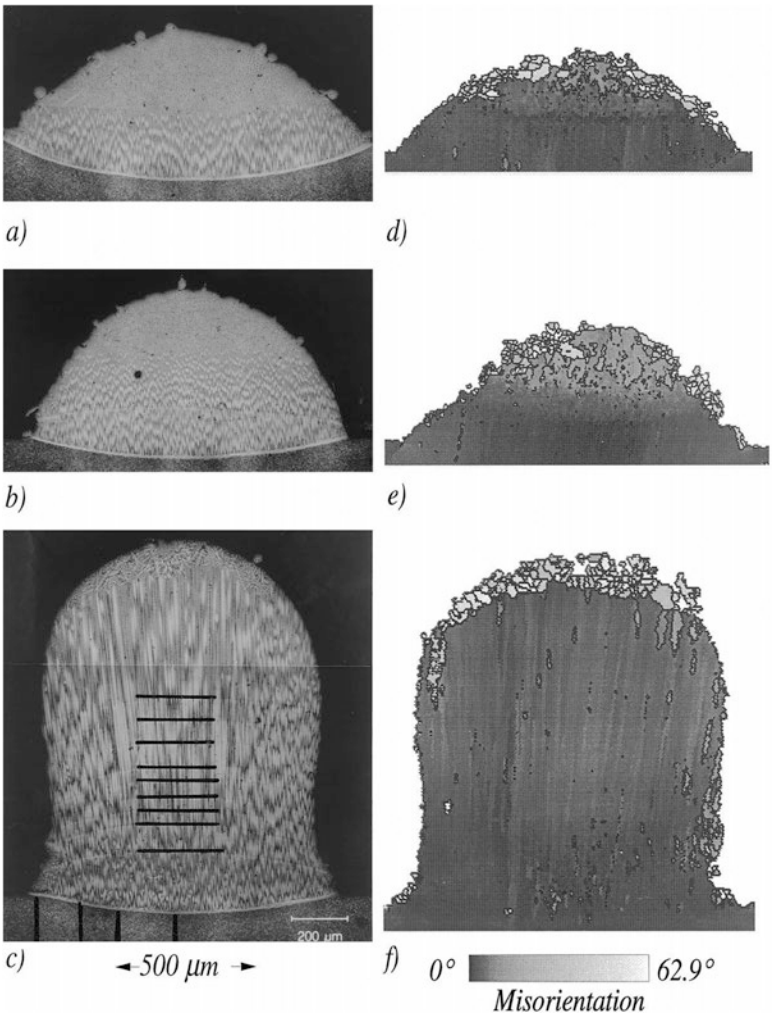

Fig. 5.7 (**a**–**c**) Optical micrographs of a transverse section of a laser formed plate-like deposit after one, two, and ten layers, respectively. (**d**–**f**) Corresponding electron backscattered diffraction (EBSD) grain structure maps

can increase from 42.0% to 48.3% as the laser scanning speed is increased from 5 mm/s to 10 mm/s. As shown in Fig. 5.10d, the height ratio of epitaxial columnar dendritic has a similar trend with the change of laser speed, whereas the height ratio can reach as high as 52% at a laser power of 200 W and speed of 10 mm/s. To further investigate the effect of laser power, the height ratio of columnar dendrite decreases from 44.8% to 43.0% as laser power increases from 200 W to 300 W (see Fig. 5.10b, d, which is also illustrated in Fig. 5.10f). It is also obvious that the simulation results agree reasonably well with the experimental results of the epitaxial

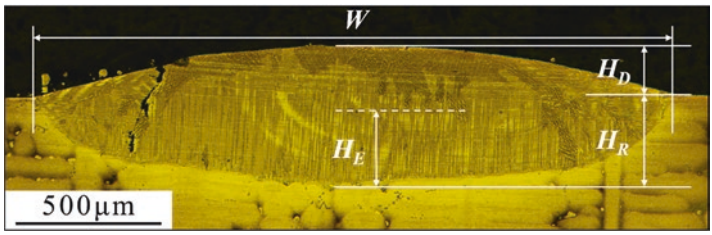

Fig. 5.8 Transverse-section microstructure of a laser cladding, i.e., a single-layer laser deposit, schematically showing several geometric dimensions crucial to SXLAM process (Liang et al. 2017a)

height ratio. According to the heat transfer simulation, the competitive growth of the grains along different crystallographic orientations can be obtained by comparing each critical CET value of $G^{3.4}/V$. Thus, the value of $G^{3.4}/V$ increases less rapidly along with the building direction at the higher laser scanning speed, which indicates the promoted epitaxial growth of columnar dendrite and the larger region of epitaxial growth. At the same time, the higher laser power can significantly decrease the thermal gradient at a higher energy input, which causes the lower value of $G^{3.4}/V$ and lower epitaxial grain height. As a result, the CET occurrence during the epitaxial growth can be directly determined by optimizing the processing parameter, and the finite element modeling of the heat transfer process provides more insights into the mechanism behind the parametric optimization.

Similar relationships between the processing parameters and the solidification conditions were also reported by Liang through the LMD of the René N5 deposit (Liang et al. 2017a). As shown in Fig. 5.11, a higher thermal gradient (G) is obtained at a lower heat input, which means the lower laser power is favorable to promote the epitaxial growth of the dendrite columnar. The solidification velocity (V) increases with early increasing laser speed (V_b) and then becomes almost unchanged with further increasing V_b. Moreover, a higher laser power (P) can further increase the solidification velocity. Wang et al. (2018) also studied the laser scanning speed on the remelted microstructure of the SX Ni-based superalloy. It is found that the equiaxed grains of [010] region are about twice as big as the area of $[0\bar{1}0]$ along the laser scanning direction on (001). Meanwhile, the primary dendritic spacing decreases with the increase of laser scanning speed, indicating a significant influence on the cooling rate during the laser remelting process.

In addition to the laser direct deposition technique, selective laser melting was also used to attempt the epitaxial growth of the SX SR999 superalloy. As another typical metal additive manufacturing technology, SLM based on the powder bed fusion possesses a higher thermal gradient, solidification velocity, and also the value of G^n/V, which makes it more likely to avoid CET during epitaxial growth of SX. From work by Yang et al. (2019), the columnar SX structure with a height of 2 mm can be obtained by using the SLM technique. Meanwhile, it should be noted that the extremely fine dendrite structure is present in the SLM SX layer with the

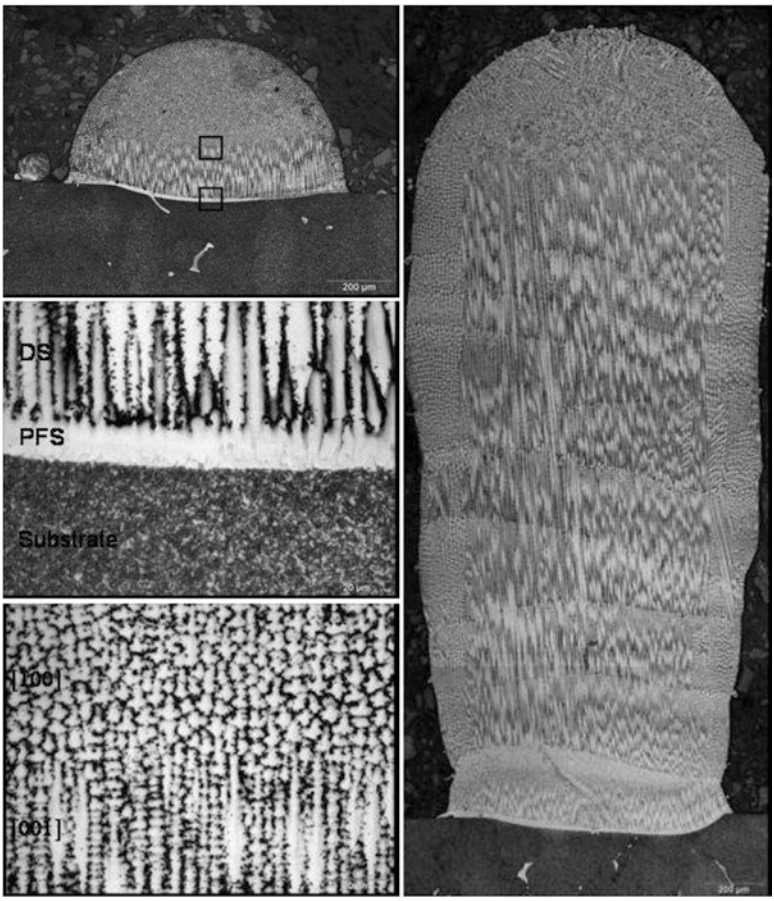

Fig. 5.9 (**a**) Cross section of a single clad; (**b**) SEM interface between the substrate and the clad; (**c**) optical micrograph of the [001]/[100] transition region (P = 500 W, v = 4 mm/s, f = 1 g/min and d = 1 mm, clad height = 495 μm); (**d**) cross section of a 10-layer deposit. The deposition direction is parallel to [100] (P = 500 W, v = 4 mm/s, f = 1 g/min and d = 1 mm, clad height = 2.5 mm) (Santos et al. 2011)

primary dendrite spacing around 1 μm and 2 μm, which is almost two orders of magnitude lower than that of the cast one (~320 μm) (see Fig. 5.12).

5.5 Influence of Substrate Conditions on Microstructure

Apart from the laser processing parameters, the condition of the SX substrate plays a crucial role in the epitaxial laser forming process. For example, the initial substrate temperature can directly influence the thermal gradient as well as the

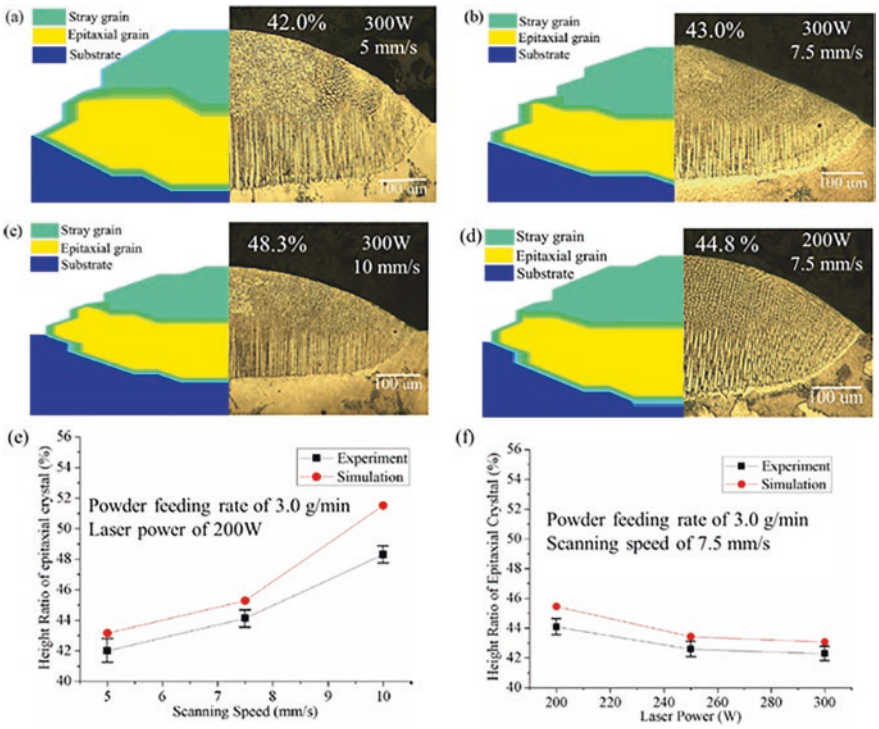

Fig. 5.10 The comparison of microstructure between the simulation and experimental deposited beads with powder feeding rate of 3.0 g/min, different laser power, and scanning speed: (**a**) 300 W, 5 mm/s; (**b**) 300 W, 7.5 mm/s; (**c**) 300 W, 10 mm/s; and (**d**) 200 W, 7.5 mm/s (Liu and Qi 2015a)

solidification velocity at the liquid/solid front and determine the grain structure during rapid solidification. Thus, the adjustment of the substrate temperature makes it possible to control the epitaxial growth of the columnar dendrite during LAM. Apart from grain structure, the misorientation of the columnar grain is another crucial factor evaluating the quality of the epitaxial deposit layer. The influence of the crystallographic orientation of the primary SX stem should be included in the study of the laser epitaxial forming process. As a result, focusing on the substrate conditions, various researches have been conducted to reveal the influence mechanism of substrate temperature and crystallographic orientation during the laser epitaxial growth process (Liu and Qi 2015b; Wang et al. 2015; Wang and Wang 2016; Liu and Wang 2018).

Liu and Wang (2018) studied the effect of initial substrate temperature on epitaxial crystal growth and microstructure formation in laser powder deposition of Ni-based SX superalloy. As shown in Fig. 5.13, it can be found that the molten pool morphology changes little as the substrate temperature increases from −30 °C to +210 °C. However, the enhanced stray grain formation and restrained epitaxial growth of columnar dendrites can be observed with the increase of substrate

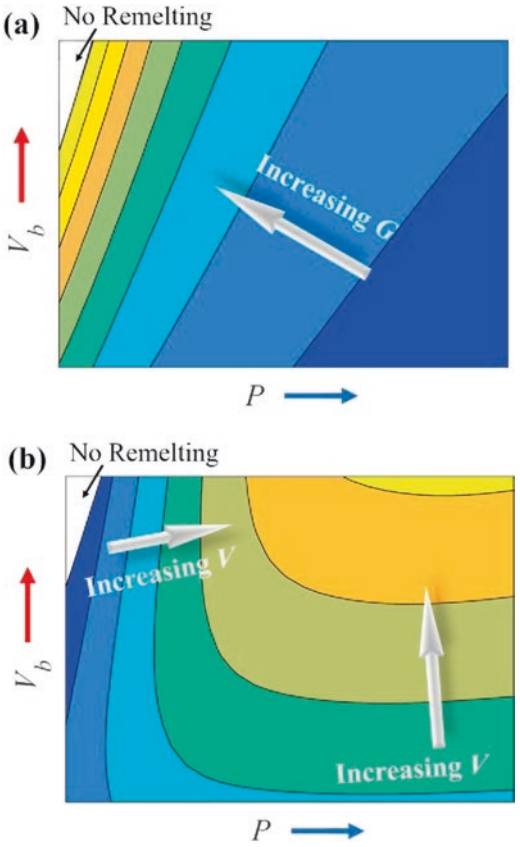

Fig. 5.11 Schematics of the variation trends of (**a**) temperature gradient G and (**b**) solidification velocity V with laser power P and scanning velocity V_b (Liang et al. 2017a)

temperature. It indicates that the lower substrate temperature can benefit the epitaxial growth of columnar dendrites and suppress the stray grain formation. At the same time, the significantly refine columnar dendrites can be found in the epitaxial deposit at a lower substrate present temperature. Such phenomena can be considered due to the enhanced $|G_{001}|^{3.4}/|V_{001}|$ ratio and weakened disturbance by molten pool fluctuation, which can in turn affect the primary dendrite arm distance. As a result, the control of the substrate provides more possibility to enhance the epitaxial growth of columnar dendrites. However, it should be noted that the high thermal gradient and cooling rate may cause more prominent cracking during the solidification of Ni-based superalloy (Qiu et al. 2019; Zhou et al. 2018). Thus, the control of thermal conditions during the laser epitaxial growth of the SX superalloy is crucial to improve the metallurgical quality.

Besides the substrate temperature, various researchers have reported the effect of crystallographic orientation on the epitaxial growth of columnar dendrites. Wang et al. (Wang et al. 2015; Wang and Wang 2016) studied the competitive growth of the dendrites with different preferential orientations during the laser remelting process of SX substrates with different crystallographic orientations. As shown in

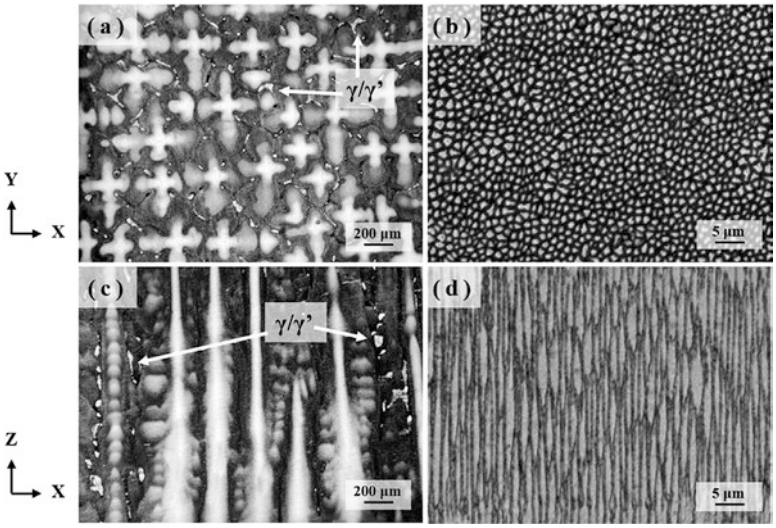

Fig. 5.12 Microstructure of the substrate and SLM sample: (**a** and **c**) horizontal and vertical microstructure of the substrate; (**b** and **d**) horizontal and vertical microstructure of SLM sample

Fig. 5.14, the crystallographic orientation of the SX stems was controlled through the rotation of the SX substrate around the axes of X and Z.

As the crystallographic orientation of the SX substrate was rotated around the x-axis by 15°, the dendritic grains formed along [0 $\bar{1}$ 0] were found to move upward at the left side of the molten pool. By further rotating the crystallographic orientation by 45° around x-axis, the [0 $\bar{1}$ 0] dendritic grains disappeared from the molten pool. The [010] dendrites have a similar tendency as the crystallographic is rotated around z-axis. The solidification structure of the molten pool was replaced by the epitaxial [001] grains at the bottom and [0 $\bar{1}$ 0] and [100] dendrites at the top. However, the area fraction of the epitaxial growth region of the SX dendrite has been hardly changed through the rotation around x- and z-axes.

It is interesting to find that the [100] dendrite gradually moves upward in the molten pool with the crystallographic orientation that is clockwise rotated around y-axis, and the region of the epitaxial [001] grains increases accordingly. As the crystallographic orientation is rotated around y-axis by 45°, the [001] dendrite is dominating the central area as a result of epitaxial growth, whereas the [100] dendrite has been eliminated. On the contrary, the boundary of [100]/[001] gradually moves downward as the crystallographic orientation was rotated around y-axis counterclockwise.

Similarly, Liu and Qi (2015b) also reported the variation of the solidification structure through the crystallographic orientation change of the SX substrate. It is found that the height ratio of the epitaxial crystal exhibits a notable increase from 9% to 94% as the inclination angle of the substrate crystallographic orientation changes from −30° to +30°. Based on the theoretical analysis (Wang et al. 2015,

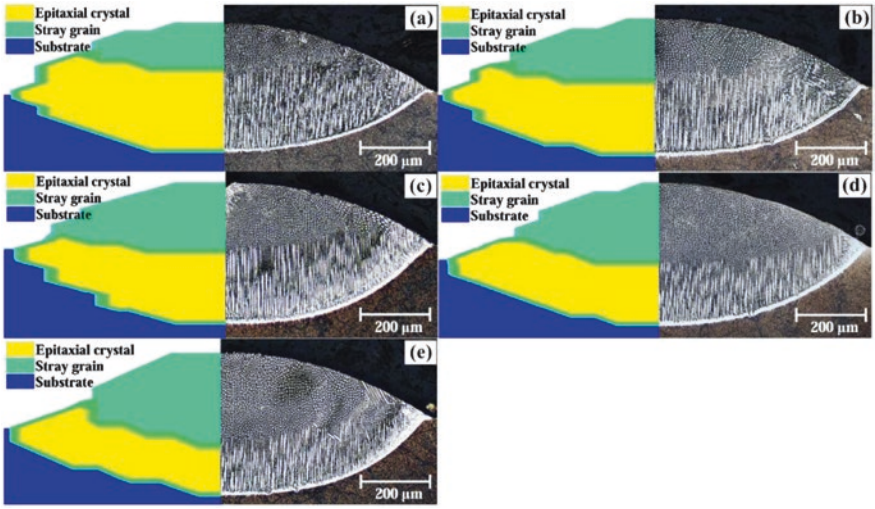

Fig. 5.13 Comparison of geometrical size and microstructure formation in the transverse section of simulation and experimental deposited bead with the Tsub = (**a**) −30 °C; (**b**) +30 °C; (**c**) +90 °C; (**d**) +150 °C; (**e**) +210 °C

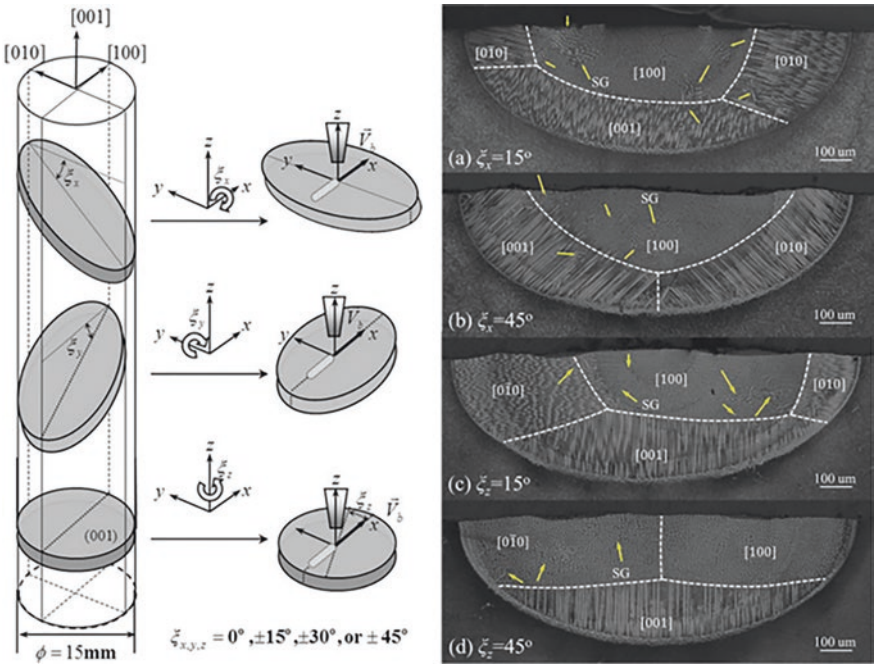

Fig. 5.14 Transverse-section micrographs for different orientations via x- and z-axis rotations

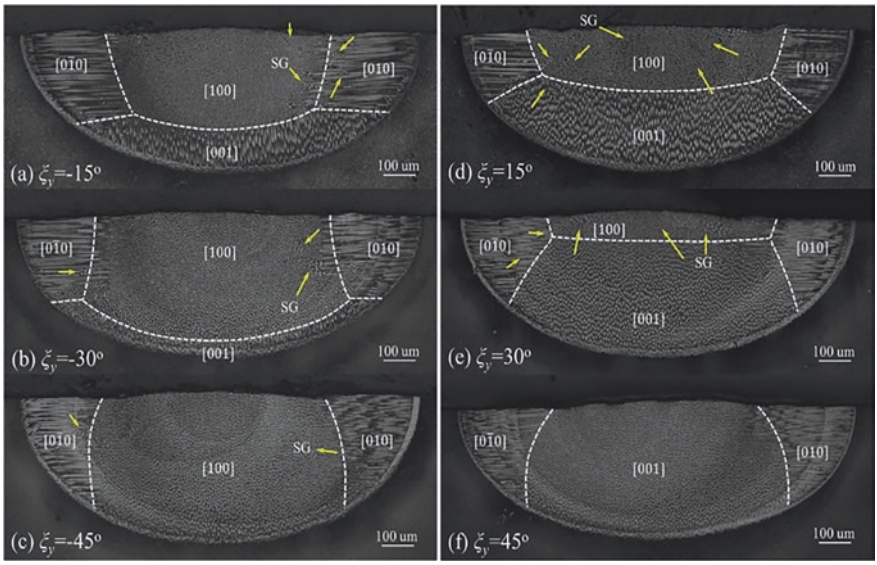

Fig. 5.15 Transverse-section micrographs for different orientations via *y*-axis rotation (Hunt 1984)

2016; Wang and Wang 2016), it can be found that the laser scanning direction toward the crystallographic orientation of the SX substrate after clockwise rotation around y-axis can produce the highest thermal gradient and promote the epitaxial growth of [001] columnar dendrite. Such phenomena indicate that epitaxial growth can be significantly influenced and promoted by controlling the crystallographic orientation of the SX substrate (Figs. 5.14 and 5.15).

5.6 Crack Formation Mechanism

With the increased demand for high-temperature mechanical properties, the Ni-based superalloy is designed and produced with increasing alloying elements to achieve the better γ' strengthening and solid solution strengthening. However, the varying melting temperature of the alloying elements to obtain such high γ' volume fractions is usually non-weldable. It also increases the difficulty of the laser-based additive manufacturing process. Especially, the majority of heavily alloyed Ni-based superalloy often suffers from cracking during the LAM process, which has become one of the main restrictions from its further application. Apart from the control of dendrite growth, the controlling of crack development has become another major issue for the LAM fabrication of single-crystal superalloy. Currently, various efforts have been made to investigate the cracking development and understand the cracking mechanisms during LAM of Ni-based superalloys.

Currently, the liquation cracking and solidification cracking are widely accepted as two primary mechanisms for crack development of Ni-based superalloys (Qiu et al. 2019; Zhou et al. 2018). Solidification cracking that is also known as the hot cracking usually occurs under the high contraction stress at the terminal stage of solidification above the solidus as a result of its low ductility. Meanwhile, the liquation cracking happens typically in the heat-affected zone of the already deposited layers, where the cyclic thermal history can cause the remelting of eutectic phases. Both types of cracking require the presence of liquid films.

In the direct laser-deposited Inconel 718 alloy, the liquation cracking is found along with low-melting-point Laves phase at grain boundaries (Chen et al. 2016; Nie et al. 2014). Similarly, the low-temperature ($\gamma + \gamma'$) eutectics along GBs are found to be responsible for the liquation cracking of laser-deposited Inconel 738 alloy (Zhong et al. 2005). In a low-carbon version of Inconel 738 (i.e., Inconel 738LC), solidification cracking was observed instead and was attributed to the formation of low-melting-point liquid films enriched in Zr and B along GBs after SLM (Cloots et al. 2016). For laser-deposited Inconel 625, solidification cracking due to low-melting-point (γ + Laves) eutectics along GBs was reported (Hu et al. 2017). It was also suggested that high-angle GBs are particularly prone to the development of solidification cracking (Chauvet et al. 2018b; Wang et al. 2004). It was argued that the high-angle GBs with higher grain boundary energy values are more likely to create a significant critical coalescence undercooling, which may lead to consequent cracking under stress.

Zhou et al. (2018) investigated the crack formation of Ni-based single-crystal superalloy using laser powder deposition of single walls and block samples. Experimental results show that the thin-wall samples exhibited crack-free single-crystal structures with the orientation of [001] as a result of epitaxial growth from the SX substrate. On the contrary, some cracks can be found in the as-deposited block samples due to the continuous layer-by-layer heating process. The EBSD shows that the large misorientation angle at the grain boundary in the cracking regions played significant roles in the crack initiation and its further propagation. Furthermore, the solidification cracking can be formed due to the columnar interdendritic shrinkage cavities. Meanwhile, the carbides with a high melting point that is formed in the interdendritic region at the early stage of the solidification can hinder the liquid flow to fill the shrinkage. Due to the pinning of carb at the liquid-filled channel, the liquid film was easy to be torn apart during the filling process. At the same time, the interdendritic low-melting-point structure may melt in heat-affected zone to form the liquid films, and the liquid films act as the initiation of the liquation cracking. Similarly, the susceptibility of the liquation cracking will also increase with the misorientation angle increasing (Fig. 5.16).

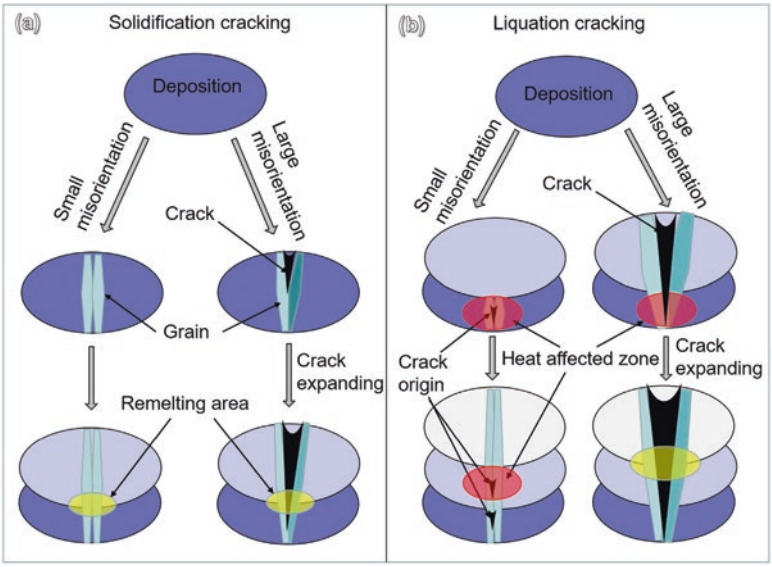

Fig. 5.16 Diagram of the cracking expanding modes. (**a**) Solidification cracking mechanism; crack formed in the region with large misorientation but not in the region with small misorientation, and it expanded during the laser remelting process. (**b**) Liquation cracking mechanism; crack origin appeared in the heat-affected zone and further cracked in the region with large misorientation, while it did not expand in the region with small misorientation (Zhou et al. 2018)

5.7 Conclusion and Perspectives

LAM technique has attracted increasing attention due to its high freedom of fabrication and design, reduction of material waste, and increase of sample complexity. Due to the small spot size and high energy density, the LAM technique can achieve the damage repair with limited heat-affected zone and low distortion caused by thermal stress. Another outstanding feature of the LAM is the ability to control the microstructure evolution by adjusting the heat transfer through the laser-related parameters. Based on the extremely high thermal gradient, the typical columnar dendrite can provide the possibility of epitaxial growth of single crystal from the SX substrate. In order to provide the potential guidance, vast efforts have been made to understand the underlying theory of epitaxial growth in LAM process and the relationship between the microstructure change and laser processing parameters. For example, the microstructure prediction has been investigated based on the model of thermal gradient and solidification, which are further understood as the laser power and scanning speed. The influence of powder feeding rate on the change of molten pool shape and the heterogeneous nuclei number are also included. Besides, the effects of the substrate conditions like columnar orientation and initial temperature have been also widely studied to ameliorate the epitaxial growth of single crystal.

However, the manufacturing of SX still remains as a major challenge for the LAM technique due to the following unsolved problems. Firstly, the precise control of the temperature field is still a major challenge during the layer-by-layer manufacturing in LAM process. The cyclic laser movement on the previously deposited layer may lead to the heat accumulation and decrease of thermal gradient and increase of solidification speed. Thus, the formation of stray grain at the top of the deposited layer is increasingly difficult to avoid with the successive buildup process, even though the partial remelting can provide the possibility of epitaxial growth. It further increases the difficulty in the manufacturing of single-crystal superalloy component with complex geometry. The control of dendrite orientation at the curved surface with specific geometry should also be accounted by manipulating the laser-related parameters. Thus, it should further enhance the understanding of rapid solidification theory in LAM process. Secondly, the development of cracking is another fact hindering the fabrication of high-quality SX superalloy by LAM technique. Besides, the segregation of alloying elements with various melting points should be accounted during the rapid solidification process of LAM. Such segregation may affect the precipitation of carbides and intermetallic compounds within the matrix material. Furthermore, the heat treatment study of the LAM SX superalloys should be made to achieve the homogenization and precipitation hardening. At last, the mechanical properties in room-temperature and high-temperature period should be investigated to reveal the distinct features of LAM SX superalloys.

References

Acharya, R., Bansal, R., Gambone, J. J., & Das, S. (2014). A microstructure evolution model for the processing of single-crystal alloy CMSX-4 through scanning laser epitaxy for turbine engine hot-section component repair (Part II). *Metallurgical and Materials Transactions B, 45*(6), 2279–2290.

Anderson, T. D., DuPont, J. N., & DebRoy, T. (2010). Origin of stray grain formation in single-crystal superalloy weld pools from heat transfer and fluid flow modeling. *Acta Materialia, 58*(4), 1441–1454.

Basak, A., & Das, S. (2016). Epitaxy and microstructure evolution in metal additive manufacturing. *Annual Review of Materials Research, 46*(1), 125–149.

Chauvet, E., Tassin, C., Blandin, J.-J., Dendievel, R., & Martin, G. (2018a). Producing Ni-base superalloys single crystal by selective electron beam melting. *Scripta Materialia, 152*, 15–19.

Chauvet, E., Kontis, P., Jägle, E. A., Gault, B., Raabe, D., Tassin, C., Blandin, J.-J., Dendievel, R., Vayre, B., Abed, S., & Martin, G. (2018b). Hot cracking mechanism affecting a non-weldable Ni-based superalloy produced by selective electron beam melting. *Acta Materialia, 142*, 82–94.

Chen, Y., Lu, F., Zhang, K., Nie, P., Elmi Hosseini, S. R., Feng, K., & Li, Z. (2016). Dendritic microstructure and hot cracking of laser additive manufactured Inconel 718 under improved base cooling. *Journal of Alloys and Compounds, 670*, 312–321.

Cloots, M., Uggowitzer, P. J., & Wegener, K. (2016). Investigations on the microstructure and crack formation of IN738LC samples processed by selective laser melting using Gaussian and doughnut profiles. *Materials and Design, 89*, 770–784.

Dadbakhsh, S., Hao, L., & Kruth, J. P. (2014). Selective laser melting towards manufacture of three dimensional in situ Al matrix composites: A review. In *High value manufacturing: Advanced research in virtual and rapid prototyping* (pp. 303–308).

DebRoy, T., Wei, H. L., Zuback, J. S., Mukherjee, T., Elmer, J. W., Milewski, J. O., Beese, A. M., Wilson-Heid, A., De, A., & Zhang, W. (2018). Additive manufacturing of metallic components – Process, structure and properties. *Progress in Materials Science, 92*(Supplement C), 112–224.

Gäumann, M., Henry, S., Cléton, F., Wagnière, J. D., & Kurz, W. (1999). Epitaxial laser metal forming: Analysis of microstructure formation. *Materials Science and Engineering A, 271*(1), 232–241.

Gäumann, M., Bezençon, C., Canalis, P., & Kurz, W. (2001). Single-crystal laser deposition of superalloys: Processing–microstructure maps. *Acta Materialia, 49*(6), 1051–1062.

Gu, D. D., Meiners, W., Wissenbach, K., & Poprawe, R. (2013). Laser additive manufacturing of metallic components: Materials, processes and mechanisms. *International Materials Review, 57*(3), 133–164.

Han, Q., Gu, Y., Setchi, R., Lacan, F., Johnston, R., Evans, S. L., & Yang, S. (2019). Additive manufacturing of high-strength crack-free Ni-based Hastelloy X superalloy. *Additive Manufacturing, 30*, 100919.

Herzog, D., Seyda, V., Wycisk, E., & Emmelmann, C. (2016). Additive manufacturing of metals. *Acta Materialia, 117*, 371–392.

Hosseini, E., & Popovich, V. A. (2019). A review of mechanical properties of additively manufactured Inconel 718. *Additive Manufacturing, 30*, 100877.

Hu, Y. L., Lin, X., Yu, X. B., Xu, J. J., Lei, M., & Huang, W. D. (2017). Effect of Ti addition on cracking and microhardness of Inconel 625 during the laser solid forming processing. *Journal of Alloys and Compounds, 711*, 267–277.

Hunt, J. D. (1984). Steady state columnar and equiaxed growth of dendrites and eutectic. *Materials Science and Engineering, 65*(1), 75–83.

Inaekyan, K., Kreitcberg, A., Turenne, S., & Brailovski, V. (2019). Microstructure and mechanical properties of laser powder bed-fused IN625 alloy. *Materials Science and Engineering A, 768*, 138481.

King, W., Anderson, A., Ferencz, R., Hodge, N., Kamath, C., Khairallah, S., & Rubenchik, A. (2015). Laser powder bed fusion additive manufacturing of metals; physics, computational, and materials challenges. *Applied Physics Reviews, 2*(4), 041304.

Kong, D., Ni, X., Dong, C., Zhang, L., Yao, J., Man, C., Wang, L., Xiao, K., & Li, X. (2019). Anisotropic response in mechanical and corrosion properties of hastelloy X fabricated by selective laser melting. *Construction and Building Materials, 221*, 720–729.

Körner, C. (2016). Additive manufacturing of metallic components by selective electron beam melting – A review. *International Materials Review, 61*(5), 361–377.

Kou, S. (2003). *Welding metallurgy* (pp. 431–446). Hoboken: Wiley.

Kurz, W., Giovanola, B., & Trivedi, R. (1986). Theory of microstructural development during rapid solidification. *Acta Metallurgica, 34*(5), 823–830.

Li, N., Huang, S., Zhang, G., Qin, R., Liu, W., Xiong, H., Shi, G., & Blackburn, J. (2019). Progress in additive manufacturing on new materials: A review. *Journal of Materials Science and Technology, 35*(2), 242–269.

Liang, Y.-J., Li, A., Cheng, X., Pang, X.-T., & Wang, H.-M. (2016). Prediction of primary dendritic arm spacing during laser rapid directional solidification of single-crystal nickel-base superalloys. *Journal of Alloys and Compounds, 688*, 133–142.

Liang, Y.-J., Li, J., Li, A., Cheng, X., Wang, S., & Wang, H.-M. (2017a). Experimental optimization of laser additive manufacturing process of single-crystal nickel-base superalloys by a statistical experiment design method. *Journal of Alloys and Compounds, 697*, 174–181.

Liang, Y.-J., Cheng, X., Li, J., & Wang, H.-M. (2017b). Microstructural control during laser additive manufacturing of single-crystal nickel-base superalloys: New processing–microstructure maps involving powder feeding. *Materials and Design, 130*, 197–207.

Liu, Z., & Qi, H. (2014). Mathematical modeling of crystal growth and microstructure formation in multi-layer and multi-track laser powder deposition of single-crystal superalloy. *Physics Procedia, 56*, 411–420.

Liu, Z., & Qi, H. (2015a). Effects of processing parameters on crystal growth and microstructure formation in laser powder deposition of single-crystal superalloy. *Journal of Materials Processing Technology, 216*, 19–27.

Liu, Z., & Qi, H. (2015b). Effects of substrate crystallographic orientations on crystal growth and microstructure formation in laser powder deposition of nickel-based superalloy. *Acta Materialia, 87*, 248–258.

Liu, S., & Shin, Y. C. (2019). Additive manufacturing of Ti6Al4V alloy: A review. *Materials and Design, 164*, 107552.

Liu, Z., & Wang, Z. (2018). Effect of substrate preset temperature on crystal growth and microstructure formation in laser powder deposition of single-crystal superalloy. *Journal of Materials Science and Technology, 34*(11), 2116–2124.

Luo, S., Huang, W., Yang, H., Yang, J., Wang, Z., & Zeng, X. (2019). Microstructural evolution and corrosion behaviors of Inconel 718 alloy produced by selective laser melting following different heat treatments. *Additive Manufacturing, 30*, 100875.

Nie, P., Ojo, O. A., & Li, Z. (2014). Numerical modeling of microstructure evolution during laser additive manufacturing of a nickel-based superalloy. *Acta Materialia, 77*, 85–95.

Qiu, C., Chen, H., Liu, Q., Yue, S., & Wang, H. (2019). On the solidification behaviour and cracking origin of a nickel-based superalloy during selective laser melting. *Materials Characterization, 148*, 330–344.

Ren, Y. M., Lin, X., Fu, X., Tan, H., Chen, J., & Huang, W. D. (2017). Microstructure and deformation behavior of Ti-6Al-4V alloy by high-power laser solid forming. *Acta Materialia, 132*, 82–95.

Santos, E. C., Kida, K., Carroll, P., & Vilar, R. (2011). Optimization of laser deposited Ni-based single crystal superalloys microstructure. *Advanced Materials Research, 154-155*, 1405–1414.

Vilar, R., & Almeida, A. (2015). Repair and manufacturing of single crystal Ni-based superalloys components by laser powder deposition – A review. *Journal of Laser Applications, 27*(S1), S17004.

Vitek, J. M. (2005). The effect of welding conditions on stray grain formation in single crystal welds – Theoretical analysis. *Acta Materialia, 53*(1), 53–67.

Wang, X., & Chou, K. (2017). Effects of thermal cycles on the microstructure evolution of Inconel 718 during selective laser melting process. *Additive Manufacturing, 18*, 1–14.

Wang, L., & Wang, N. (2016). Effect of substrate orientation on the formation of equiaxed stray grains in laser surface remelted single crystal superalloys: Experimental investigation. *Acta Materialia, 104*, 250–258.

Wang, N., Mokadem, S., Rappaz, M., & Kurz, W. (2004). Solidification cracking of superalloy single- and bi-crystals. *Acta Materialia, 52*(11), 3173–3182.

Wang, L., Wang, N., Yao, W. J., & Zheng, Y. P. (2015). Effect of substrate orientation on the columnar-to-equiaxed transition in laser surface remelted single crystal superalloys. *Acta Materialia, 88*, 283–292.

Wang, G. W., Liang, J. J., Zhou, Y. Z., Jin, T., Sun, X. F., & Hu, Z. Q. (2016). Effects of substrate crystallographic orientations on microstructure in laser surface-melted single-crystal superalloy: Theoretical analysis. *Acta Metallurgica Sinica-English Letters, 29*(8), 763–773.

Wang, G., Liang, J., Yang, Y., Shi, Y., Zhou, Y., Jin, T., & Sun, X. (2018). Effects of scanning speed on microstructure in laser surface-melted single crystal superalloy and theoretical analysis. *Journal of Materials Science and Technology, 34*(8), 1315–1324.

Yan, M., Dargusch, M. S., Ebel, T., & Qian, M. (2014). A transmission electron microscopy and three-dimensional atom probe study of the oxygen-induced fine microstructural features in as-sintered Ti–6Al–4V and their impacts on ductility. *Acta Materialia, 68*, 196–206.

Yan, X., Yin, S., Chen, C., Huang, C., Bolot, R., Lupoi, R., Kuang, M., Ma, W., Coddet, C., Liao, H., & Liu, M. (2018). Effect of heat treatment on the phase transformation and mechanical

properties of Ti6Al4V fabricated by selective laser melting. *Journal of Alloys and Compounds, 764*, 1056–1071.

Yan, X., Yin, S., Chen, C., Jenkins, R., Lupoi, R., Bolot, R., Ma, W., Kuang, M., Liao, H., Lu, J., & Liu, M. (2019). Fatigue strength improvement of selective laser melted Ti6Al4V using ultrasonic surface mechanical attrition. *Materials Research Letters, 7*(8), 327–333.

Yang, J., Li, F., Pan, A., Yang, H., Zhao, C., Huang, W., Wang, Z., Zeng, X., & Zhang, X. (2019). Microstructure and grain growth direction of SRR99 single-crystal superalloy by selective laser melting. *Journal of Alloys and Compounds, 808*, 151740.

Zhong, M., Sun, H., Liu, W., Zhu, X., & He, J. (2005). Boundary liquation and interface cracking characterization in laser deposition of Inconel 738 on directionally solidified Ni-based superalloy. *Scripta Materialia, 53*(2), 159–164.

Zhou, Z., Huang, L., Shang, Y., Li, Y., Jiang, L., & Lei, Q. (2018). Causes analysis on cracks in nickel-based single crystal superalloy fabricated by laser powder deposition additive manufacturing. *Materials and Design, 160*, 1238–1249.